Research article

Insights of the formation mechanism of nanostructured titanium oxide polymorphs from different macromolecular metal-complex precursors

Patricio Allende [a], Alodia Orera [b], Miguel Á. Laguna-Bercero [b,*], María Luisa Valenzuela [c], Carlos Díaz [d], Lorena Barrientos [e,f]

[a] Departamento de Química, Universidad Católica del Norte, Avda Angamos, 0610, Antofagasta, Chile
[b] Instituto de Nanociencia y Materiales de Aragón (INMA), CSIC-Universidad de Zaragoza, 50009, Zaragoza, Spain
[c] Universidad Autónoma de Chile, Institute of Applied Chemical Sciences, Inorganic Chemistry and Molecular Materials Group, Facultad de Ingeniera, Porvenir 580, Edificio L, Primer Piso, Temuco, Chile
[d] Departamento de Química, Facultad de Química, Universidad de Chile, La Palmeras 3425, Nuñoa, Casilla, 653, Santiago de Chile, Chile
[e] Facultad de Química y de Farmacia, Centro de Investigación en Nanotecnología y Materiales Avanzados CIEN-UC, Pontificia Universidad Católica de Chile, Vicuña Mackenna, 4860, Macul, Santiago de Chile, Chile
[f] Millennium Nuclei on Catalytic Processes Towards Sustainable Chemistry (CSC), Chile

ARTICLE INFO

ABSTRACT

The insight into the mechanism of the unprecedented formation of pure anatase TiO$_2$ from the macromolecular (Chitosan)•(TiOSO$_4$)$_n$ precursor has been investigated using micro Raman spectroscopy, Scanning Electron Microscopy (SEM) and thermogravimetric/differential thermal analysis (TGA/DTA). The formation of a graphitic film was observed upon annealing of the macromolecular precursor, reaching a maximum at about 500 °C due to decomposition of the polymeric chain of the Chitosan and (PS-co-4-PVP) polymers. The proposed mechanism is the nucleation and growth of TiO$_2$ nanoparticles over this graphitic substrate. SEM and Raman measurements confirm the formation of TiO$_2$ anatase around 400 °C. The observation of an exothermic peak around 260 °C in the TGA/DTA measurements confirms the decomposition of carbon chains to form graphite. Another exothermic peak around 560 °C corresponds to the loss of additional carbonaceous residues.

1. Introduction

Among the different nanoparticle fabrication methods, solid-state pyrolysis has gained much importance in recent years [1, 2, 3]. Although solution synthesis methods generally permit the control of the particle's size and morphology [4, 5, 6], the incorporation of as-prepared nanoparticles into solid-state devices for practical applications [7, 8, 9, 10] is not straightforward [11], as solution phase methods usually imply nanoparticle agglomeration [12, 13, 14]. On the other hand, solid-state preparation methods usually allow an easy and direct incorporation of particles into solid-state matrices such as SiO$_2$, TiO$_2$ Al$_2$O$_3$ and even glasses. For example, we have previously reported a novel solid-state method to synthesize metallic nanostructures from pyrolysis at 800 °C of metallic and organometallic derivatives of poli- and oligophosphazene [15, 16, 17, 18, 19]. Other complex nanostructure precursors of physical state mixtures such as MLn/[NP(O$_2$C$_{12}$H$_8$)]$_3$ were also reported [20, 21, 22]. However, in several of these systems the sought M (or M$_x$O$_y$) phase is

accompanied by a phosphate byproduct phase [23]. Consequently, in order to obtain directly the pure M or M$_x$O$_y$ phase, it is necessary to use a P free polymer template. In this sense, we have recently developed a novel method using macromolecular Chitosan•MXn and PS-co-4-PVP•MXn precursors followed by subsequent solid-state pyrolysis at 800 °C under air [23, 24, 25, 26].

However, although the formation of nanoparticles in solution is well known [27, 28, 29], the studies of solid-state preparation methods are limited, and the parameters controlling both the size and the morphology of the formed nanoparticles are unknown [18]. In this regard, we have evidenced that the pyrolysis of the precursor {NP(OC$_8$H$_{12}$)$_2$ (OC$_6$H$_4$PPh$_2$-Mn(CO)$_2$ (η^5-C$_5$H$_4$Me)$_2$} occurs through the intermediate formation of a layered graphite host which is formed in the first step of the thermal solid-state reaction [18].

Titanium dioxide (TiO$_2$) is a well-known semiconductor, which can crystallize in eight different polymorphic forms [30] e.g. rutile, anatase, brookite, TiO2–B (bronze). In particular, anatase is known to be a

---

potential solar-driven photocatalyst active for the photodegradation of various dye contaminants [31]. The photocatalytic performance of TiO_2 largely depends on its physical and chemical properties such as morphology, surface area and crystallinity [32, 33]. In this context, solid state methods to prepare pure TiO_2 phase are a constant challenge [11], with mainly two different solid-state methods reported in the literature [34, 35]. Dodd et al. [34] prepared a mixture of anatase and brookite powder by solid-state chemical reaction of anhydrous $TiOSO_4$ with Na_2CO_3. Besides, Gillan et al. synthesized rutile from solid-state metathesis reaction of $TiCl_3$ with Na_2O_2 [35]. Also TiO_2 nanoparticles were prepared using solid-state methods [36, 37], however it was not possible to isolate the anatase phase.

Recently, we have also reported a solid-state method to prepare pure anatase phase by selecting the adequate precursor from different macromolecular complexes [38]. As described in this work, different combinations of anatase/rutile could be achieved depending on the used precursor, with pure anatase phase finally achieved by a two-step method with the $(Chitosan) \bullet (TiOSO_4)_n$ precursor after pyrolysis at 800 °C. The obtained TiO_2 nanostructures present a very efficient photocatalytic decoloration in a short time. The best photocatalyst degrades methylene blue (MB) by 98 % in only 25 min measured at 655 nm, in an alkaline medium. These results (showed the most efficient photocatalyst reported in the literature, in a short time, using pure TiO_2 without the addition of any other phase or dopant [39, 40]. An extended comparison of the photocatalytic response of different TiO_2 nanoparticles was performed [38]. Moreover, the factors controlling their photocatalytic properties are the size and then the crystal phase and subsequently the morphology. It is also remarkable that these three aforementioned factors have not been controlled simultaneously. In any case, the formation mechanism of TiO_2 is still unknown. In the present work, we report some insight about the formation mechanism of TiO_2 from different macromolecular complexes: $(Chitosan) \bullet (TiLn)$ (I), $(PS-co-4-PVP) \bullet (TiLn)$ with $TiLn = Cp_2TiCl_2$, $TiOSO_4$ and $TiO(acac)_2$ organometallic or metallic salt of Ti. Raman spectroscopy, Scanning Electron Microscopy (SEM) and thermogravimetric/differential thermal analysis (TGA/DTA) techniques at temperatures between 250 °C to 800 °C were used to elucidate the changes that occur in the precursors during their annealing.

2. Experimental

2.1. Precursors

The synthesis and characterization of the macromolecular complexes $(Chitosan) \bullet (Cp_2TiCl_2)$ **(I)**, $(PS-co-4-PVP) \bullet (Cp_2TiCl_2)$ **(II),** $(Chitosan) \bullet (TiOSO_4)$ **(III)** $(PS-co-4-PVP) \bullet (TiOSO_4)$ **(IV)** $(Chitosan) \bullet (Ti (acac)_2)$ **(V),** y $(PS-co-4-PVP) \bullet (Ti (acac)_2)$ **(VI)** were prepared as previously as described in reference [38].

Chitosan, Poly (styrene-co-4-vinylpyridine), Cp_2TiCl_2, $TiOSO_4$, $TiO(acac)_2$ were used as received from Sigma-Aldrich.

2.2. Thermogravimetric analysis (TGA/DTA)

Thermogravimetic analysis was performed using both a DTA-TGA SDT-2960 instrument (TA Instruments) at the Institute of Nanoscience and Materials of Aragon (INMA), and a TGA4000, 100–240V/50–60Hz (Perkin Elmer) at the Institute of Applied Chemical Sciences of the Autonomous University of Chile.

2.3. Raman spectroscopy

Raman scattering measurements were performed using a DILOR XY spectrometer with a CCD detector and a spectral resolution of 1.4 cm^{-1}.

The 514.53 nm line of an argon ion laser (Ar^+) was used as a source of excitation. Dispersed light was collected through an x50 microscope objective lens. A Linkam TS1500V stage was used for in situ thermal treatments. Raman spectra were fitted with 2 gaussian-like peaks using OriginPro software, with R^2 values above 0.9 obtained in all cases. The integrated intensity of each peak was ascribed to D and G modes respectively.

2.4. Morphological characterization

Scanning Electron Microscopy (SEM) analysis was performed using a Merlin Field Emission SEM (Carl Zeiss, Germany) in order to analyse the morphology of the particles from the different precursors.

2.5. Pyrolysis of macromolecular complexes

In order to obtain the nanostructured TiO_2, macromolecular complexes were pyrolyzed in a porcelain crucible using a furnace (model LEF-105S-1, LabTech) under air atmosphere at 500 °C, 600 °C, 700 °C and 800 °C for 4 h, and using a heating rate of 10 °C/min.

3. Results and discussion

A detailed Raman analysis of the different samples was performed. We have clear evidences of the formation of anatase and/or rutile phases as summarized in the appendix. Here we will focus on the formation of carbon species in order to elucidate the nucleation of TiO2 particles since, as based on the literature, it is believed that a graphitic layer plays a crucial role on the nanoparticle formation. The precursors **(I), (II), (III), (IV), (V),** and **(VI)** were annealed at 400 °C and their Raman spectra are shown in Figure 1, where the typical D and G graphite bands [18, 41, 42, 43, 44] are observed. These bands are not clearly defined in some cases, as observed for the macromolecular precursor **(III)** and **(V).** This is a consequence of an incomplete combustion of the polymer leading to organic C–H residues. These D and G bands have been previously reported for the combustion of the macromolecular complex {NP(O-$C_8H_{12})_2(OC_6H_4PPh_2-Mn(CO)_2$ (η^5-$C_5H_4Me)_2$} where the formation of graphitic particles was observed [18].

The formation of other carbon species as graphene has been also observed in thermal treatments of metal-dextran gel materials [45]. In this sense, it has been suggested that the carbon species are probably formed from the carbon chains skeleton of the polymeric metal macromolecular complexes [46]. For instance, based on preceding studies, soluble metallic precursors have been reported using graphitic materials such as graphite, graphene and carbon nanotubes as templates to deposit metal nanoparticles. . It is believed that the metal nanoparticles are covalently bound to the graphite surface, as most chemical reactions occur by reduction or functionalization. As an example, selective deposition of iron oxide on highly oriented pyrolytic graphite using iron chloride as a precursor was recently reported [47]. Selective deposition is happening on the defects and step edges of the graphite, producing iron oxide nanoparticles without any additional chemical treatments. These authors also suggested a mechanism for the deposition and conversion of iron hydroxides and oxyhydroxides into iron oxide by air annealing, in a similar mechanism as the one presented in this work.

The broadened bands and enhanced intensity in the "D" band, exhibited by the Raman spectra in Figure 1, are typical of nanocrystalline graphite [48, 49].

Detailed in situ Raman measurements as a function of the temperature were performed in order to get information of the TiO₂ formation mechanism. Raman spectra were recorded from 200 °C at intervals of 50 °C for the macromolecular complex **(VI)**, and then it was annealed up to
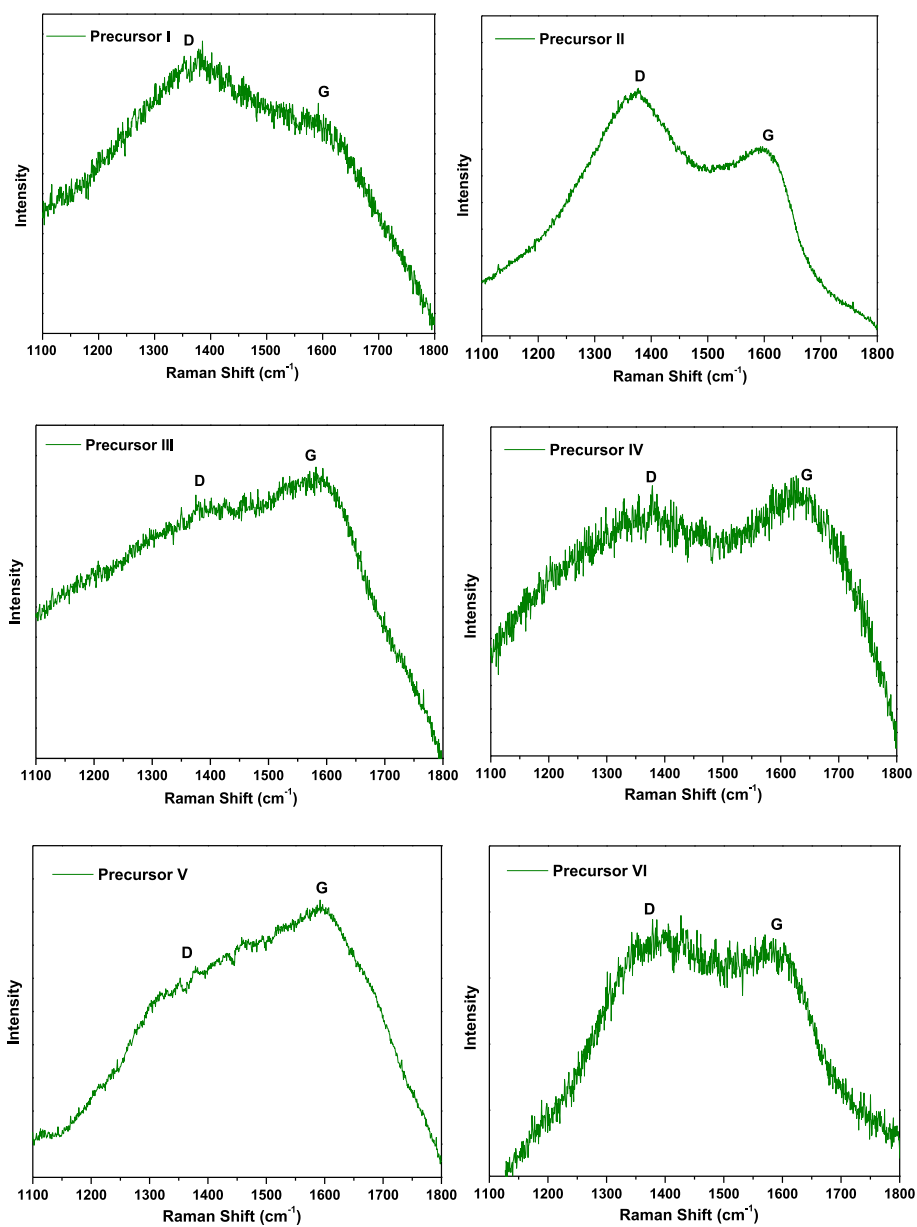
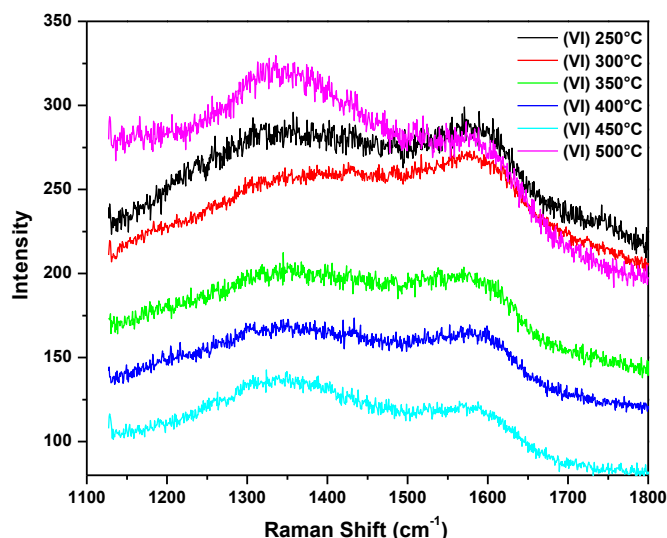**Figure 1.** Raman spectra in the zone of the D and G bands for the precursors (I)-(VI) pyrolized at 400 °C.

Figure 2. Raman spectra in the zone of the D and G bands for the precursor (VI) pyrolyzed at 250 °C, 300 °C, 350 °C, 400 °C, 450 °C and 500 °C.
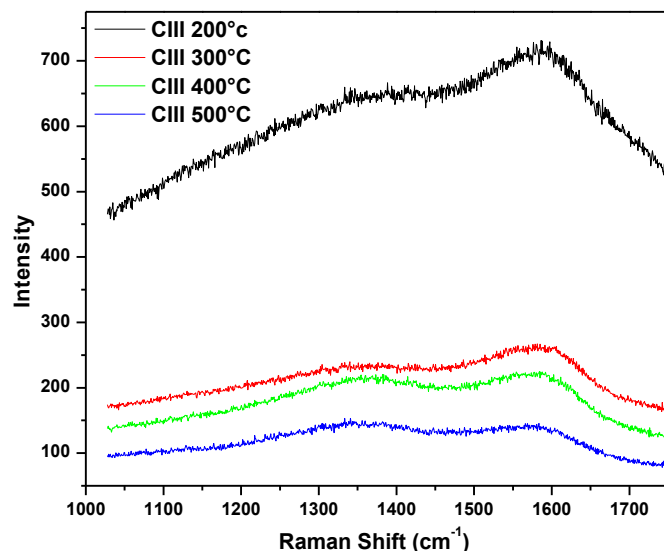

Figure 4. Raman spectra in the zone of the D and G bands for the precursor (III) pyrolyzed at 200 °C, 300 °C, 400 °C, and °C 500 °C.

500 °C (see Figure 2). The formation of graphitic layers becomes evident at 250 °C. When increasing the temperature, the intensity of the D band increases and the G band decreases up to 500 °C, where the D band becomes most intense.

The graphitization degree can be expressed by the I_D/I_G ratio. Diverse values in the same sample suggest a high degree of inhomogeneity of the material during the pyrolytic process, being this a typical behavior for this material [11, 17]. From these experiments, an increase of the formation of non-graphitic materials is observed (I_D/I_G increase) from 250 °C to 450 °C. Above this temperature, an increase of the graphitization degree I_D/I_G was observed due to carbonization (see Figure 3). The behavior up to 450 °C is consistent with the thermal conduct of some polymers [45], where graphene or graphitic materials are formed during annealing. Above this temperature ie. from 500 °C to 800 °C this graphitic template disappears by a combustion process to give mainly CO_2 and H_2O.

The evolution of the Raman spectra of **(III)** as a function of temperature is observed in Figure 4, where a similar behavior was found. Both D

and G bands appear at 200 °C, suggesting the formation of a graphitic phase. At 400 °C, the maximum intensity was found for the D band, and finally at 500 °C both D and G bands become less intense due to carbonization near to the total loss of organic matter.

For precursor (III), the variation of I_D/I_G with the temperature, indicate a maximum in the formation of the non-graphite phase at 400 °C following by a decrease of the I_D/I_G ratio (see Figure 5). This maximum indicates an increase of the formation of a graphitic template materials, where the nanoparticles of anatase begin to nucleate and then a decreasing of these graphitic materials on raising the temperature, suggesting their lost as CO_2 over 400 °C, then following to 800 °C where the carbon is lost almost completely.

The nucleation of metal oxide nanoparticles in the form of needle or bars, as previously reported for III and IV precursors [38], was confirmed by SEM. As observed in Figure 6, when the calcination temperature is increased, TiO_2 nanoparticles nucleate forming bars of about 2–10 μm in length. Those microfibers are composed of agglomerated nanoparticles of 20–30 nm, as seen in Figure 6e for precursor III. We believe that the
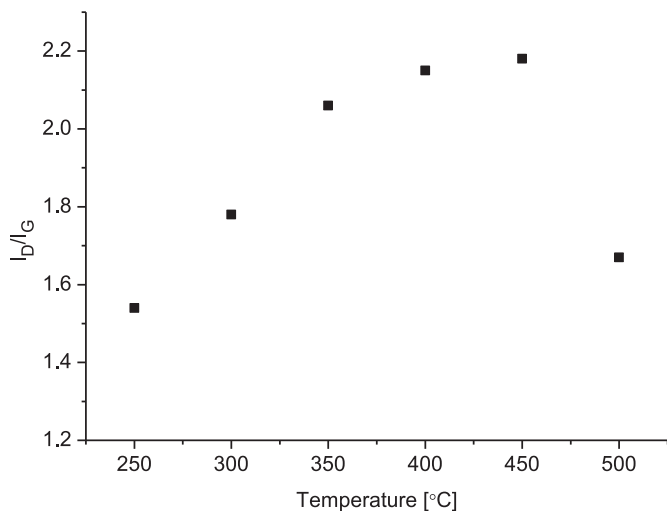

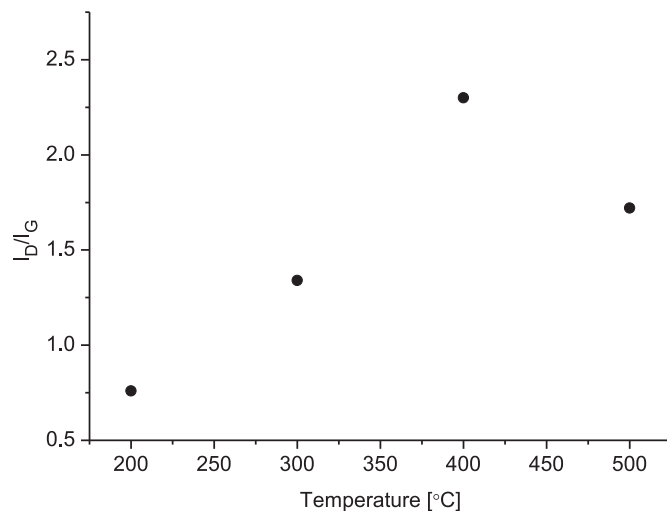**Figure 3.** I_D/I_G ratios vs temperature for the pyrolytic product **(VI)**.

Figure 5. I_D/I_G ratios vs temperature for the pyrolytic product **(III)**.
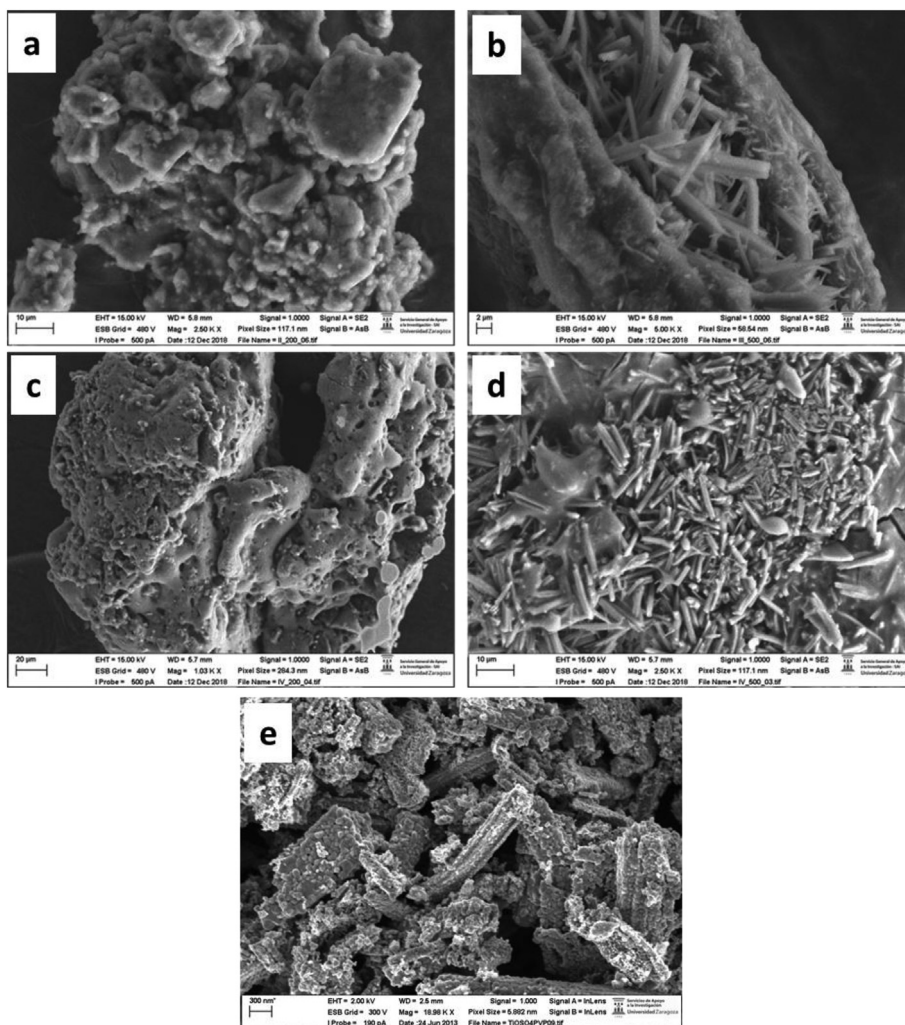
Figure 6. SEM micrographs showing the morphology of the calcined products under different conditions: (a) precursor III calcined at 200 °C; (b) precursor III calcined at 500 °C; (c) precursor IV calcined at 200 °C; (d) precursor IV calcined at 500 °C; and (e) precursor III after full calcination.

presence of $TiOSO_4$ linked to the polymeric chain, for TiO_2(III) and TiO_2(IV) precursors, induces the formation of microfibers formed by fused nanoparticles on the surface, leading to large surface areas (as seen in Figure 6). This seems to be independent of the polymer and pyrolysis temperature. The observation of needle-like agglomerated TiO_2 nanoparticles is in concordance with the results reported by Wang et al. In

their studies, the titanium glycolate precursor $Ti(OCH_2CH_2O)_2$ was synthesized using a solvothermal route. Pure anatase phase was obtained after oxidation. The authors claimed that the organic ligands at the surface of the chains prevented the agglomeration of the chains during calcination., In addition, they found a chain-shape change with large specific surface area [50]. In our case, the organic ligands of the chitosan
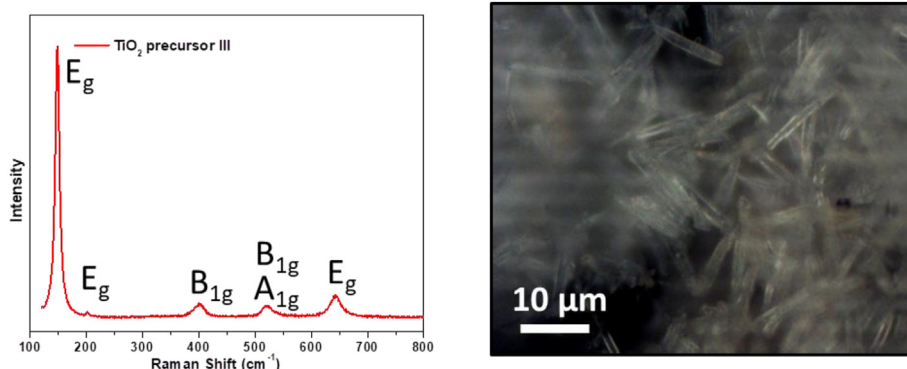
Figure 7. Raman spectrum (left) of the area show in the optical image (right), which corresponds to the TiO_2 precursor (III).

and PVP linked to the $TiOSO_4$ also prevent the aggregation in a similar manner, thus forming the needle-like agglomerated TiO_2 nanoparticles.

Interestingly, from Raman spectra in the zone of both D and G bands for the precursors (I)-(V) and in the zone of the anatase and rutile phase of TiO_2 with temperature, the formation of the anatase phase can be observed already at temperatures of 200 °C for precursors I, II, V, and VI, as shown in detail in the appendix. An intense peak at 150 cm^{-1} confirms the presence of anatase in precursor III. The presence or rutile in precursors I and II, and in minor proportion in IV, was confirmed as an intense peak at 600 cm^{-1}. As an example, the Raman spectrum of the anatase phase and the corresponding analyzed area for precursor III is shown in Figure 7. A complete study of all the precursors can be found in the appendix. We can then conclude that anatase/rutile mixture phases are being formed at 800 °C for the precursors I and II. In addition, pure anatase single phase is formed for the precursors III, IV, V, and VI. In our previous work, it was found that the precursor polymers play a key role during the nucleation process of the TiO_2 into the anatase or rutile phase [38]. However, this step was not completely elucidated. They confirmed band gap energies higher than bulk values by the study of the absorption edge, which are in concordance with the quantum confinement effect of smaller TiO_2 nanostructures. On the other hand, the tendencies regarding the crystal phase are in agreement with the previously reported band gap energies. In any case, it was found no direct correlation of the morphology with E_g values.

A thermogravimetric analysis (TGA) of both the macromolecular complexes and the polymer was previously carried out and presented in the supplementary information of reference [38], in order to obtain information about the thermal process during the combustion. However, this TGA information is now very relevant and needs direct correlation with the findings already discussed regarding Raman spectroscopy. For example, for the III and IV precursors, three clear weight losses were observed. The ones related to carbon species are the second peak at 260–320 °C, attributed to the decomposition of carbons where the species NH_2, CH_2OH and OH are found; and finally the third peak at 500–600 °C associated to the carbonization of organic matter equivalent to the central ring of chitosan (precursor III) and the styrene group in the polymer and the sulphate group in the metal precursor forming SO_2 (precursor IV). Specifically for precursor IV, the peak displacement was assigned to the decomposition of the pyridine group, confirming the coordination of the titanium to the polymer chain. The presence of two peaks, could be due to the combustion of the pyridine group coordinated to the metallic precursor $TiOSO_4$ (297 °C), while at 325 °C occurs the calcination of the pyridine group without coordination. Similar findings were reported by Chaudhary et al. [51] using related coordinated polymers. They found a two-step decomposition at 300 °C and 335 °C, which can be related with our observations for the PVP compound. We can then correlate that the decomposition of the second peak at 260–300 °C is consistent with the formation of graphite as observed by Raman spectroscopy starting at 250 °C. The carbonization associated with the third decomposition peak is also consistent with the decrease of both D and G bands observed at 500 °C, which become less intense due to carbonization of the remaining organic matter.

A tentative mechanism for the formation of TiO_2 nanoparticles is proposed, suggesting that at the intermediate pyrolysis temperature (300–500 °C) a graphitic surface is formed, being crucial for the growth of TiO_2 nanoparticles. The further increase up to 800 °C leads to graphite decomposition, although some carbon traces are remaining as a shell coating of the TiO_2 nanoparticles.

4. Conclusions

Raman studies on the thermal treatment of the TiO_2 precursors (Chitosan)•(Cp$_2$TiCl$_2$) **(I)**, (PS-co-4-PVP)•(Cp$_2$TiCl$_2$) **(II)**, (Chitosan)•($TiOSO_4$) **(III)** (PS-co-4-PVP)•($TiOSO_4$) **(IV)** (Chitosan)•(Ti (acac)$_2$) **(V)**, y (PS-co-4-PVP)•(Ti (acac)$_2$) **(VI)** at several temperatures confirmed the formation of a graphitic thin layer around 500 °C, where the TiO_2 nanoparticles grow up.

After this temperature, SEM images show the formation of bars composed of agglomerated TiO_2 nanoparticles. TGA/DTA analysis confirmed an exothermic peak around 500 °C assigned to the combustion of the organic matter of the respective polymer template thus producing holes where the TiO_2 nanoparticles grow-up. Raman spectra of the precursors confirm the formation of anatase, which already begins to be observed at 200 °C.

Declarations

Author contribution statement

Patricio Allende: Performed the experiments; Analyzed and interpreted the data; Wrote the paper.

Alodia Orera, Miguel Á. Laguna-Bercero, María Luisa Valenzuela, Carlos Díaz, Lorena Barrientos: Conceived and designed the experiments; Performed the experiments; Analyzed and interpreted the data; Contributed reagents, materials, analysis tools or data; Wrote the paper.

Funding statement

Data availability statement

Data will be made available on request.

Declaration of interests statement

The authors declare no conflict of interest.

### Additional information

No additional information is available for this paper.

APPENDIX

Raman spectra of precursors (I) to (VI). For each precursor, the Raman spectra were performed at three temperatures: 200 °C, 400 °C and 800 °C. (a,c,e). Next to each Raman image appears an optical microscope image, taken on the zone were the Raman spectra were performed (b,d,f). In the figure e and for some precursors (I,II, IV and VI) more than one spectrum was recorded to find the best Raman response. The same situation occurs for the Raman spectrum at 200 °C (figure a for each the precursors II, IV and V). A strong band around 150 cm^{-1} indicate the presence of TiO_2 anatase while a strong band at 600 cm^{-1} confirm the presence TiO_2 rutile.
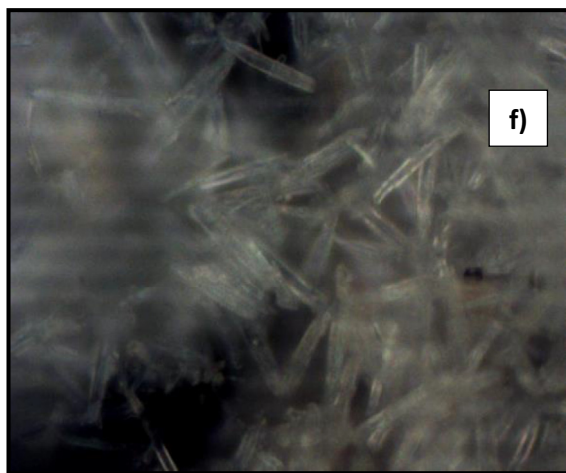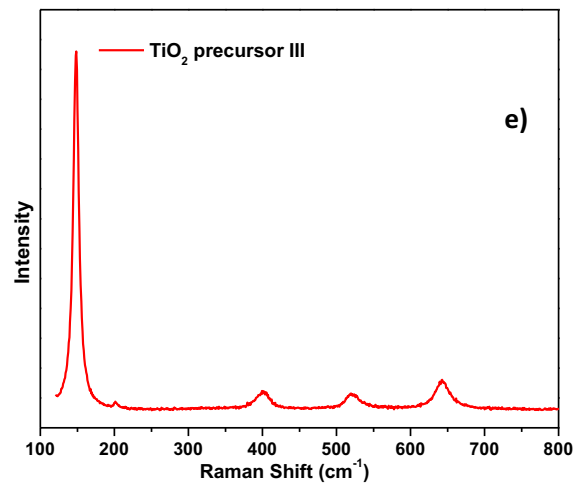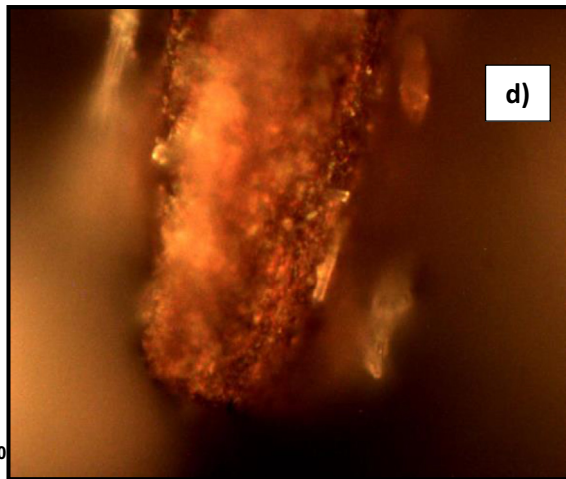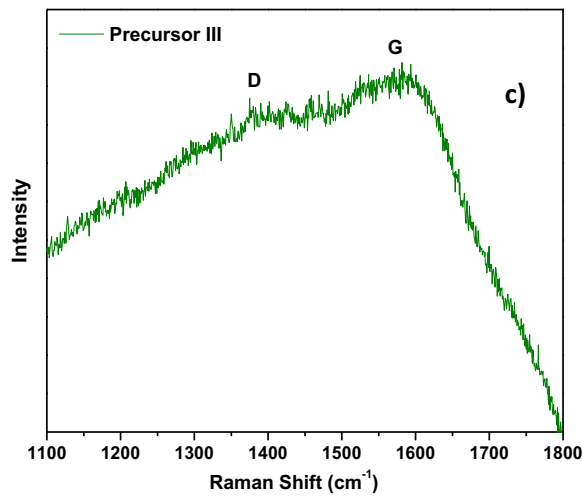
Precursor I
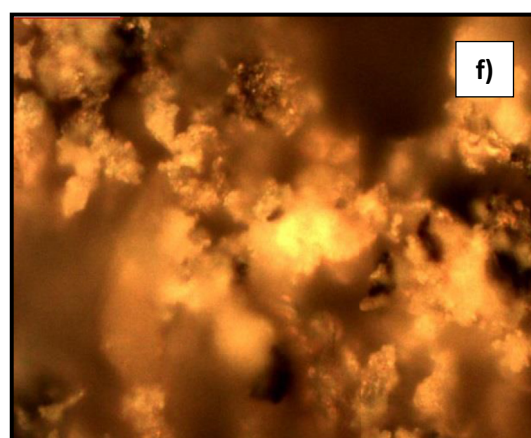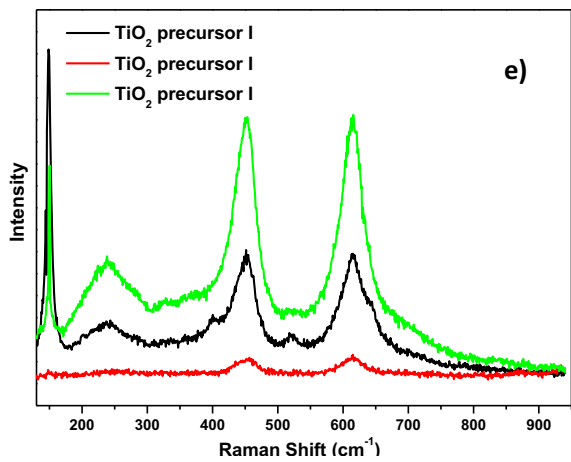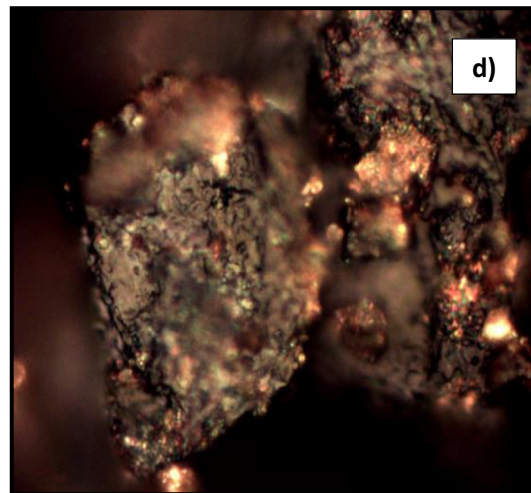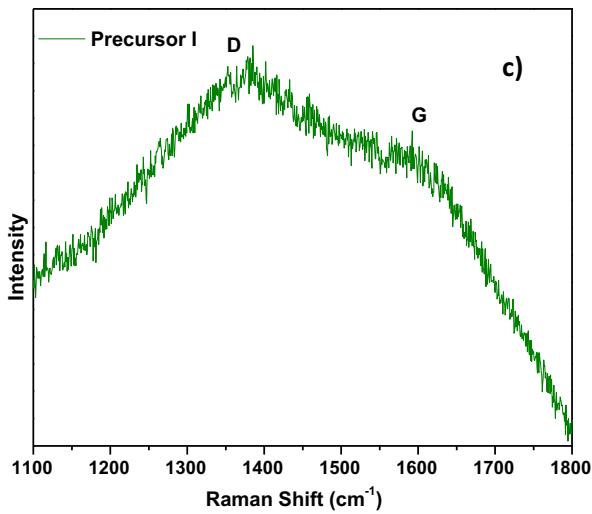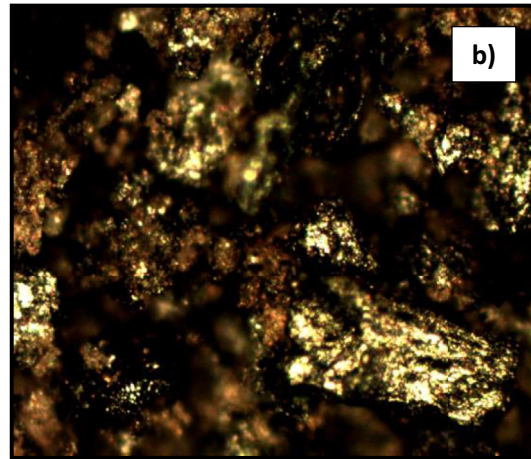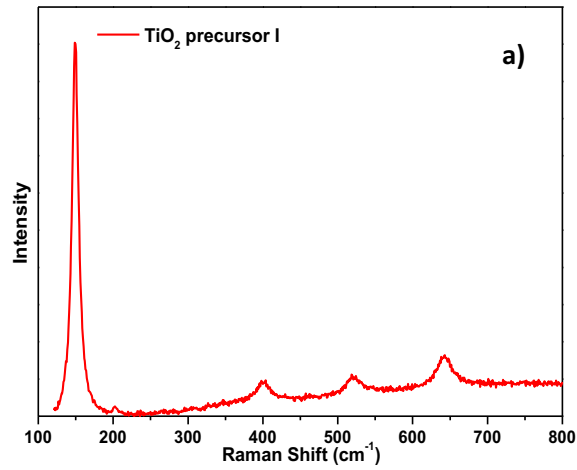
Precursor II
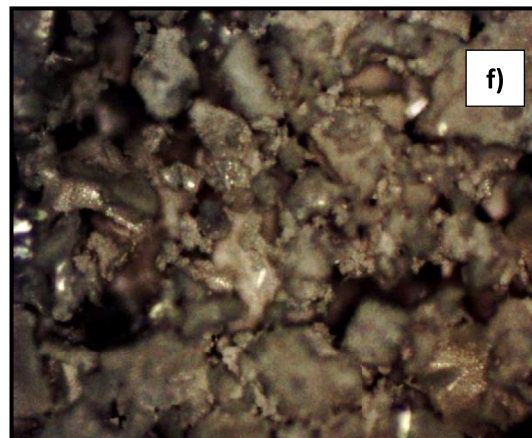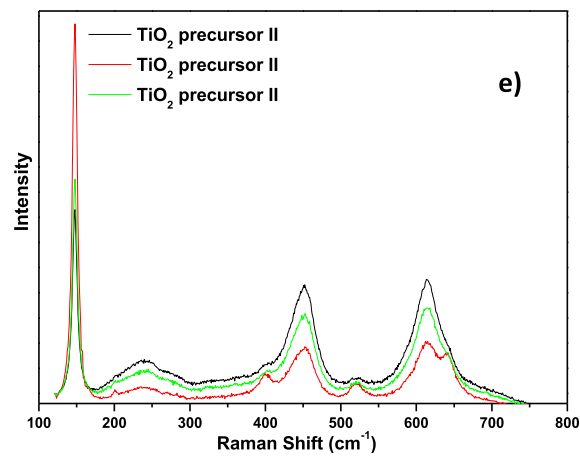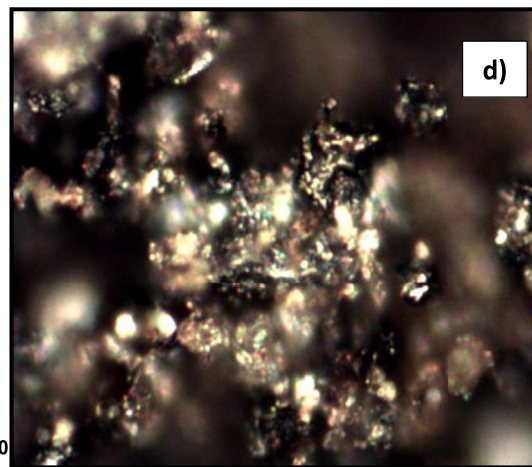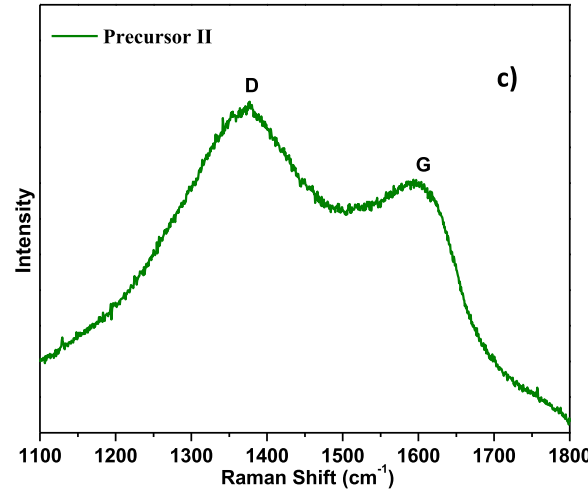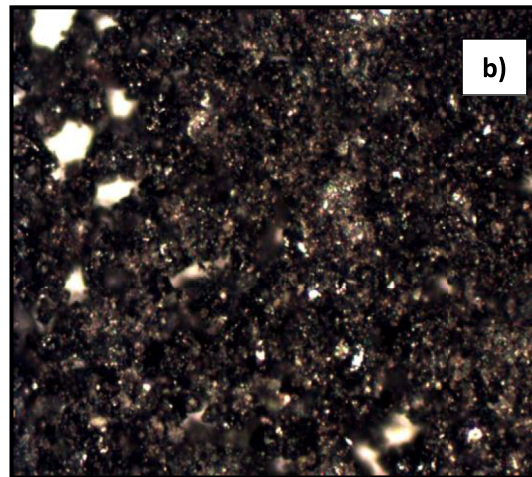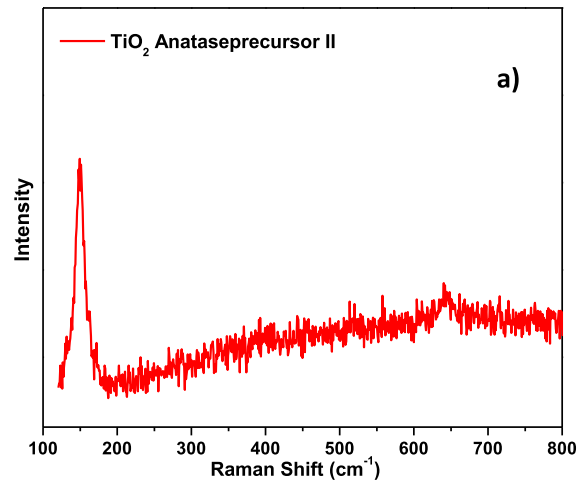
Precursor III
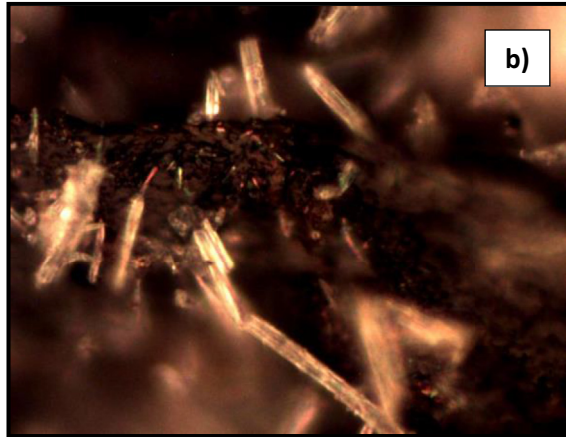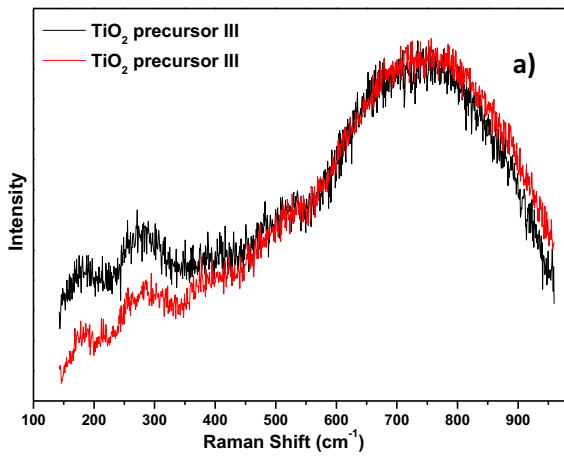
Precursor IV
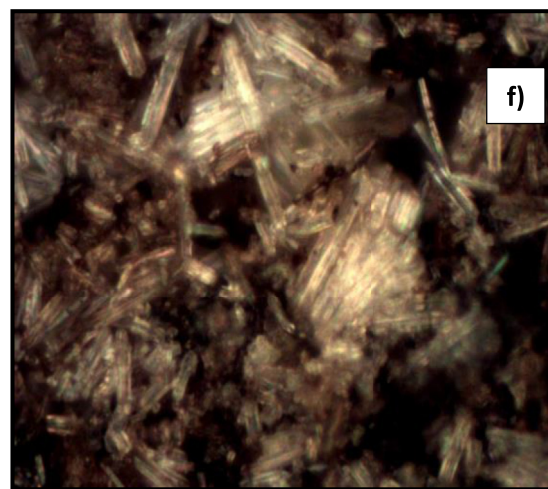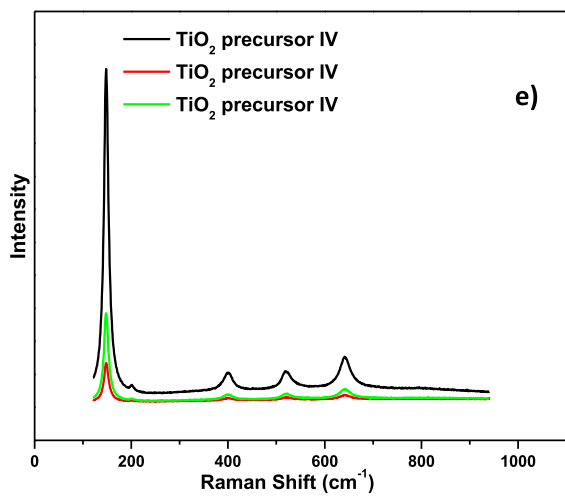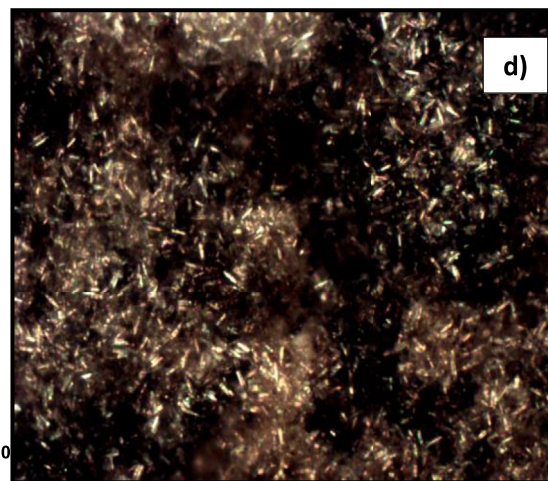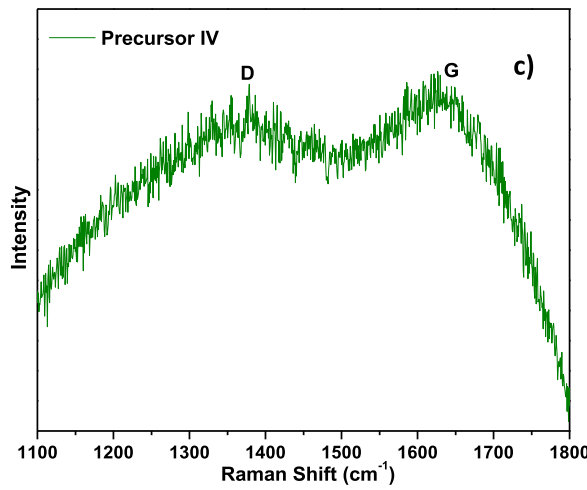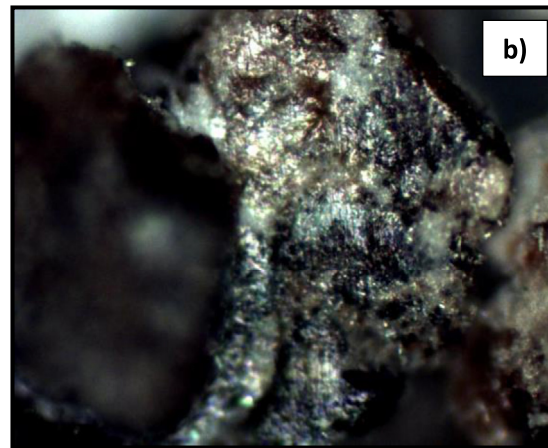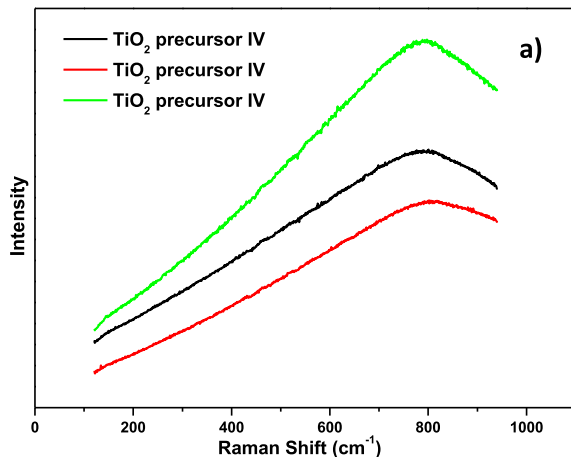
Precursor V
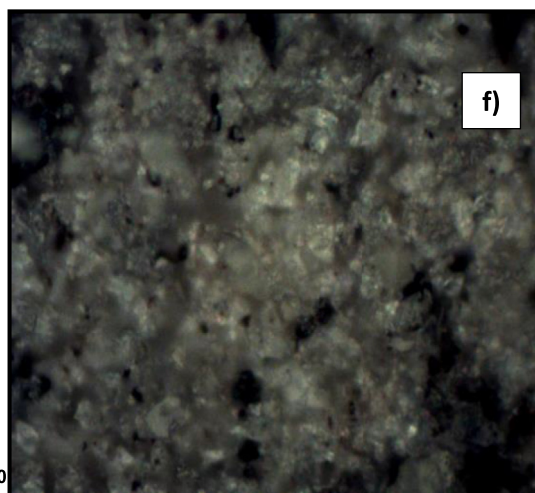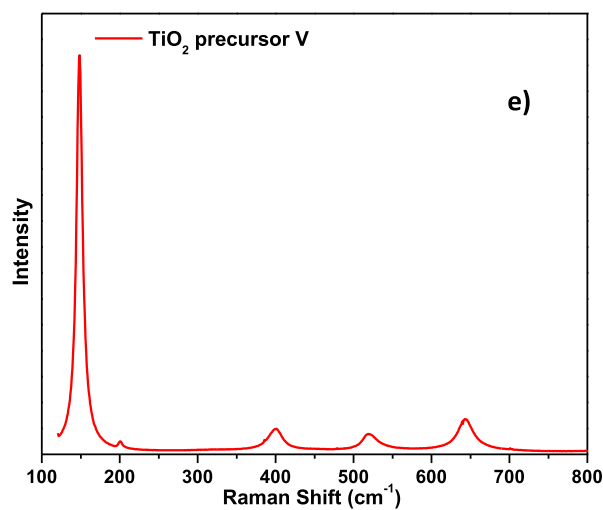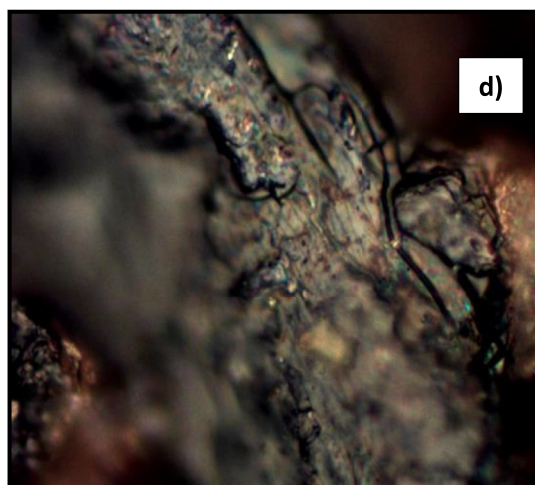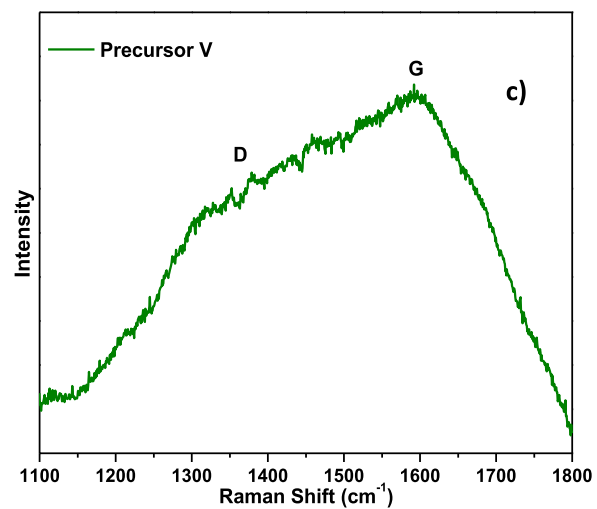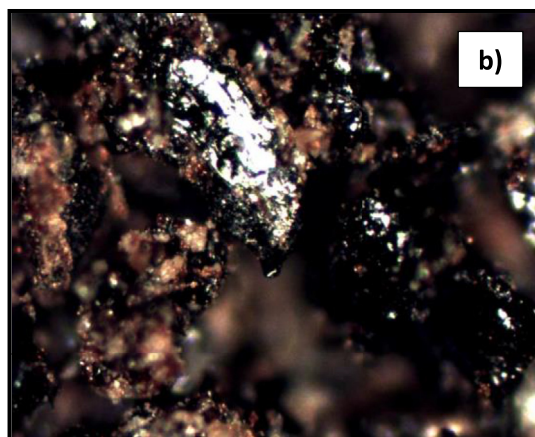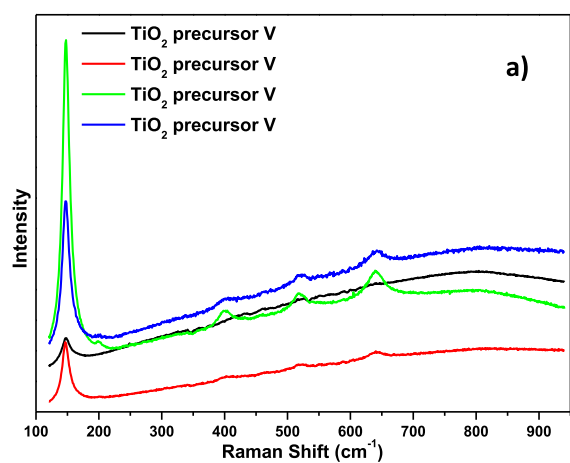
Precursor VI
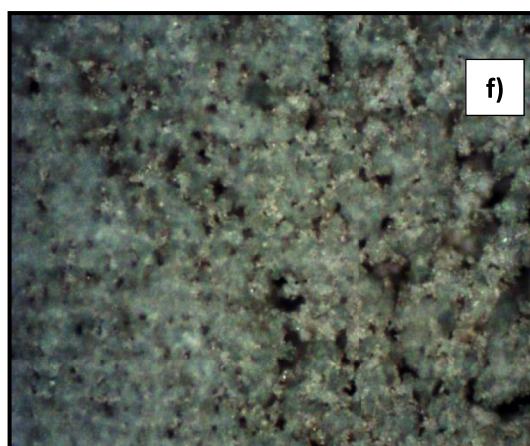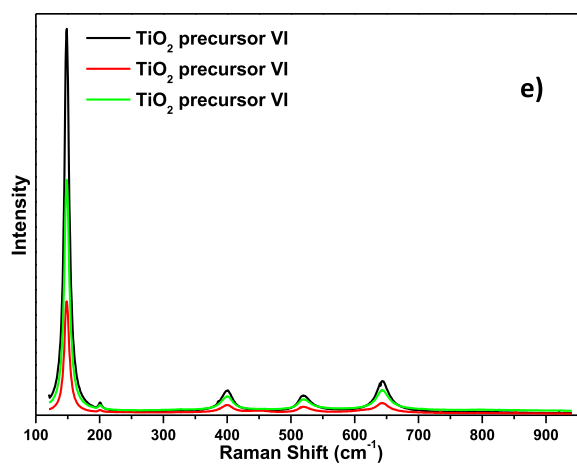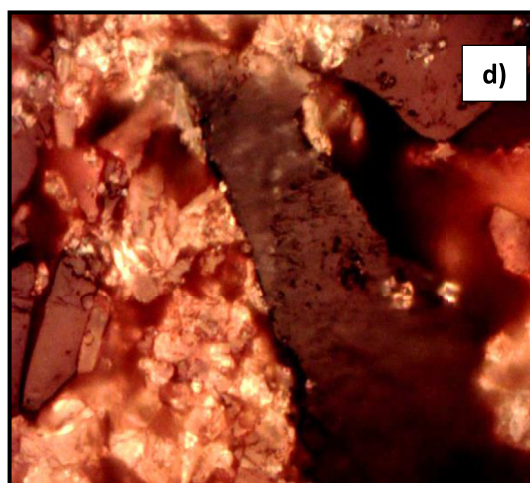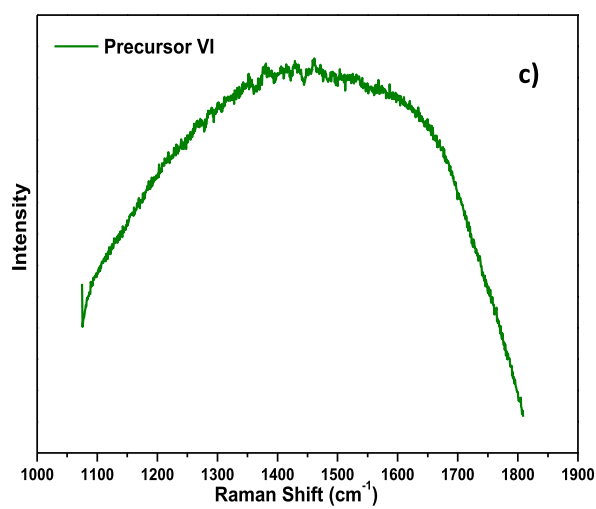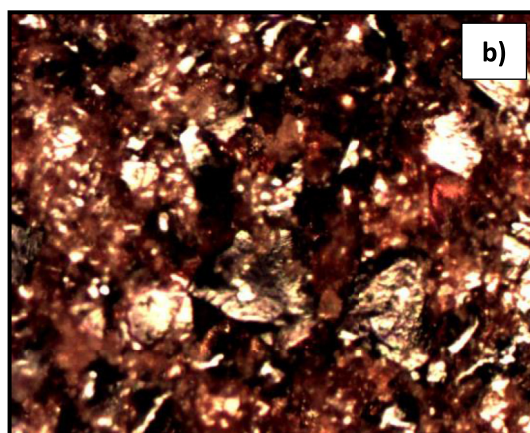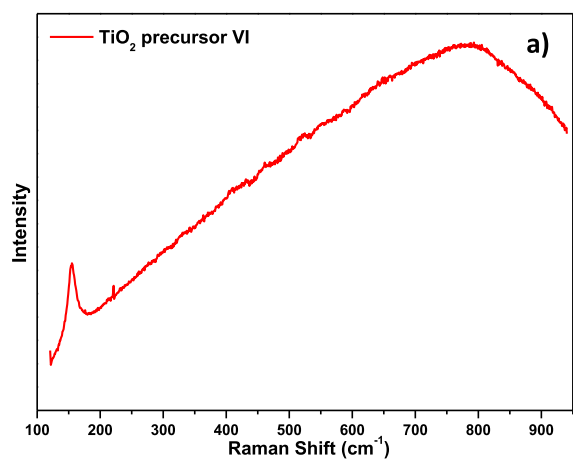
References

[1] C.N. Rao, A. Muller A, A.K. Cheetham, The Chemistry of Nanomaterials, Wiley VCH, Weinheim, 2004.

[2] S. Teranishi, T. Hasegawa, M. Shimizu, M. Miyake, Heat induced size evolution of gold nanoparticles in the solid state, Adv. Mater. 13 (2001) 1699–1701.

[3] Y. Ju-Nam, J.R. Lead, Manufactured nanoparticles: an overview of their chemistry, interactions and potential environmental implications, Sci. Total Environ. 400 (2008) 396–414.

[4] J. Qiu, X. Jiang, C. Zhu, M. Shirai, J. Si, N. Jiang, K. Hirao, Manipulation of gold nanoparticles inside transparent materials, Angew. Chem. Int. Ed. 43 (2004) 2230–2234.

[5] L-L Tan Wee-Jun Ong, S.-P. Chai, S.-T. Yong, A.-R. Mohamed, Highly reactive {001} facets of TiO 2-based composites: synthesis, formation mechanism and characterization, Nanoscale 6 (2014) 1946–2008.

[6] S.C. Glotzer, M.J. Solomon, Anisotropy of building blocks and their assembly into complex structures, Nat. Mater. 6 (2007) 557–562.

[7] G. Walkers, I.P. Parkin, The incorporation of noble metal nanoparticles into host matrix thin films: synthesis, characterisation and applications, J. Mater. Chem. 19 (2009) 574–590.

[8] J. Cao, Ch. Shao, S. Shengxian, F. Wan, Ch. Gao, Y. Zhao, L. Jiang abd L. Qu, Laser –assisted larged-scale fabrication of all-solid-state asymmetrical micro-supercapacitor array, Small 14 (2018) 1801809.

[9] B. Teo, X. Sun, Silicon-based low-dimensional nanomaterials and nanodevices, Chem. Rev. 107 (2007) 1454–1532.

[10] G.B. Khomutov, V.V. Kislov, M.N. Antipirina, R.V. Gainutdinov, S.P. Gubin, A. Yy Obydenov, S.A. Pavlov, A.A. Rakhnyanskaya, A.N. Sergeev-Cherenkov, E.S. Soldatov, D.B. Suyatin, A.L. Toltikhina, A.S. Trifonov, T.V. Yurova, Interfacial nanofabrication strategies in development of new functional nanomaterials and planar supramolecular nanostructures for nanoelectronics and nanotechnology, Microelectron. Eng. 69 (2003) 373–383.

[11] C. Díaz, M.L. Valenzuela, Metallic nanostructures using oligo and polyphosphazenes as template or stabilizer in solid state, Encycl. Nanosci. Nanotechnol. 16 (2010) 239–256.

[12] M.P. Pileni, Self-Assembly of inorganic nanocrystals: fabrication and collective intrinsic properties, Accounts Chem. Res. 40 (2007) 685–693.

[13] M.P. Pileni, 2D superlattices and 3D supracrystals of metal nanocrystals: a new scientific adventure, J. Math. Chem. 21 (2001) 16748–16758.

[14] Y.F. Wan, N. Goubet, P.A. Albouy, M.P. Pileni, Hierarchy in Au nanocrystal ordering in supracrystals: a potential approach to detect new physical properties, Langmuir 29 (2013) 7456–7463.

[15] C. Díaz, M.L. Valenzuela, Small-Molecule and High-Polymeric Phosphazenes containing oxypyridine side groups and their organometallic derivatives; Useful precursors for metal nanostructured materials, Macromolecules 39 (2006) 103–111.

[16] C. Díaz, M.L. Valenzuela, Organometallic derivatives of polyphosphazenes as precursors for metallic nanostructured materials, J. Inorg. Organomet. Polym. Mater. 16 (2006) 419–435.

[17] C. Díaz, M.L. Valenzuela, L. Zuñiga, C. O'Dwyer, Organometallic derivatives of cyclotriphosphazene as precursors of Nanostructured metallic materials: a new solid state Method, J. Inorg. Organomet. Polym. Mater. 19 (2009) 507–520.

[18] C. Díaz, M.L. Valenzuela, V. Lavayen, C. O'Dwyer, Layered graphitic carbon host formation during liquid-free solid state growth of metal pyrophosphates, Inorg. Chem. 51 (2009) 6228–6236.

[19] C. Díaz, M.L. Valenzuela, G.A. Carriedo, L. Zuñiga, C. O'Dwyer, Polymer/trimer/ metal complex mixtures as precursors of gold nanoparticles: tuning the morphology in the solid-state, J. Inorg. Organomet. Polym. 22 (2012) 447–454.

[20] C. Díaz, M.L. Valenzuela, S. Cáceres, C. ODwyer, Solution and surfactant-free growth of supported high index facet SERS active nanoparticles of rhenium by phase demixing, J. Mater. Chem. 1 (2013) 1566–1572.

[21] C. Díaz, M.L. Valenzuela, S. Cáceres, C. ODwyer, Solvent and stabilizer free growth of Ag and Pd nanoparticles using Metallic salts/cyclotriphosphazenes mixtures, Mater. Chem. Phys. 143 (2013) 124–132.

[22] C. Díaz, M.L. Valenzuela, L. Zuñiga, C. ODwyer, Solid state pathways to complex shape evolution and tunable porosity during metallic crystal growth, Sci. Rep. 2642 (2013) 1–8.

[23] C. Díaz, M.L. Valenzuela, V. Lavayen, K. Mendoza, O. Peña, C. O'Dwyer, Nanostructured copper oxides and phosphates from a new solid-state route, Inorg. Chim. 377 (2011) 5–13.

[24] C. Diaz, S. Platoni, A. Molina, M.L. Valenzuela, H. Geaney, C. O'Dwyer, Novel solid-state route to nanostructured tin, zinc and cerium oxides as potential materials for sensors, J. Nanosci. Nanotechnol. 14 (2014) 6748–6753.

[25] C. Diaz, L. Barrientos, D. Carrillo, J. Valdebenito, M.L. Valenzuela, P. Allende, Solvent-less method for efficient photocatalytic [small alpha]-Fe2O3 nanoparticles using macromolecular polymeric precursors, New J. Chem. 40 (2016) 6768–6776.

[26] C. Díaz, M.L. Valenzuela, M.A. Laguna-Bercero, A. Orera, D. Bobadilla, S. Abarca, O. Peña, Synthesis and magnetic properties of nanostructured metallic Co, Mn and

[27] Ni oxide materials obtained from solid-state metal-macromolecular complex precursors, RSC Adv. 7 (2017) 27729–27736.

[27] S. Mozaffari, W. Li, C. Thompson, S. Ivanov, S. Seifert, B. Lee, L. Kovarik, A. Karim, Colloidal nanoparticle size control: experimental and kinetic modeling investigation of the ligand–metal binding role in controlling the nucleation and growth kinetics, Nanoscale 9 (2017) 13772–13785.

[28] T. Nguyen, T.K. Thah, N. Maclean, S. Mahiddine, Mechanisms of nucleation and growth of nanoparticles in solution, Chem. Rev. 114 (2014) 7610–7630.

[29] E. Finney, R. Finke, Nanocluster nucleation and growth kinetic and mechanistic studies: a review emphasizing transition-metal nanoclusters, J. Colloid Interface Sci. 317 (2008) 351–374.

[30] X. Chen, S.S. Mao, Titanium dioxide nanomaterials: synthesis, properties, modifications, and applications, Chem. Rev. 107 (2007) 2891–2959.

[31] X. Liu, J. Iocozzia, Y. Wang, X.C. Cui, Y. Chen, Sh. Zhao, Z. Li Zh. Lin, Correction: inorganic-modified semiconductor TiO2 nanotube arrays for photocatalysis, Energy Environ. Sci. 10 (2017) 402–434.

[32] G. Liu, H.G. Yang, J. Pan, Y.Q. Yang, G.Q. Qing Lu, H.-M. Cheng, Titanium dioxide crystals with tailored facets, Chem. Rev. 114 (2014) 9559–9612.

[33] X. Zheng, Q. Kuang, K. Yang, Y. Qiu, J. Qiu, Sh. Yang, Mesoporous TiO2 single crystals : facile Shape-,Size, and phase controlled growth and efficient photocatalytic perfomance, ACS Appl. Mater. Interfaces 5 (2013) 11249–11257.

[34] A. Dodd, A. McKinley, T. Tsuzuki, M. Saunders, Optical and photocatalytic properties of nanocrystalline TiO2 synthesised by solid-state chemical reaction, J. Phys. Chem. Solid. 68 (2007) 2341–2348.

[35] S. Perera, N. Zelenski, E.G. Gillan, Synthesis of nanocrystalline TiO2 and reduced titanium oxides via rapid and exothermic metathesis reactions, Chem. Mater. 18 (2006) 2381–2388.

[36] S. Sh. Al-Omary, L.A. Algharagholy, M.E. Al-Dokheily, Band gap modification of Tio2 using solid state reaction with hydrides in argon atmosphere, Int. J. Eng. Technol. 7 (2018) 354–362.

[37] A. Sanchez-Martinez, C. Koop-Santa, O. Ceballos-Sanchez, Edgar R. López-Mena, M.A. González, V. Rangel-Cobián, E. Orozco-Guareño, M. García-Guaderrama, Study of the preparation of TiO2 powder by different synthesis methods Mater, Res. Express 6 (2019), 085085.

[38] P. Allende, M.A. Laguna-Bercero, L. Barrientos, M.L. Valenzuela, C. Diaz, Solid state tuning morphology, crystal phase and size through metal macromolecular complexes and its significance in the photocatalytic response, ACS Appl. Energy Mater. 1 (2018) 3159–3170.

[39] G. Wang, H. Wang, Y. Ling, Y. Tang, X. Yang, R.C. Fitzmorris, C. Wang, J.Z. Zhang, Y. Li, Hydrogen-treated TiO2 nanowire arrays for photoelectrochemical water splitting, Nano Lett. 11 (2011) 3026–3033.

[40] R. Li, Y. Weng, X. Zhou, X. Wang, Y.M. Chong, H. Han, C. Li, Y. Mi, Achieving overall water splitting using titanium dioxide-based photocatalysts of different phases, Energy Environ. Sci. 8 (2015) 2377–2378.

[41] P. Dallas, A.B. Bourlinos, Ph. Komninou, M. Karakassides, D. Niarchos, Silver nano particles and graphitic carbon through thermal decomposition of a siver/acetylenedicarboxylic salt, Nanoscale Res. Lett. 4 (2009) 1358–1364.

[42] J. Hong, M.K. Park, E. Jung Lee, DaeEung Lee, D.Seok Hawang S. Ryu, Origin of new broad Raman D and G peaks in annealed graphene, Sci. Rep. 3 (2013) 2700.

[43] J. Campos-Delgado, H. Farhat, Y.A. Kim, A. Reina, J. Kong, M. Endo, H. Muramatsu, T. Hayashi, H. Terrones, M. Terrones, M.S. Dresselhaus, Resonant Raman study on bulk and isolated graphitic nanoribbons, Small 5 (2009) 2698–2702.

[44] M. Endo, K. Nishimura, Y.A. Kim, K. Hakamada, T. Matushita, M.S. Dresselhaus, G. Dresselhaus, Raman spectroscopic characterization of submicron vapor-grown carbon fibers and carbon nanofibers obtained by pyrolyzing hydrocarbons, J. Mater. Res. 14 (1999) 4474–4477.

[45] M.K. Tynan, D.W. Johnson, B.P. Dobson, K.S. Coleman, Formation of 3D graphene foams on soft templated metal monoliths, Nanoscale 8 (2016) 13303–13310.

[46] Ch. Kim, Sang-Hee Park, Jang-Ik Cho, Do-Young Lee, Tae-Jin Park, Wan-Jin Lee, Kap-Seung Yang, Raman spectroscopic evaluation of polyacrylonitrile-based carbon nanofibers prepared by electrospinning, J. Raman Spectrosc. 35 (2004) 928–933.

[47] C. de Alwis, T.R. Leftwich, P. Mukherjee, A. Denofre, K.A. Perrine, Spontaneous selective deposition of iron oxide nanoparticles on graphite as model catalysts, Nanoscale Adv. 1 (2019) 4729–4744.

[48] D.R. Tallant, T.A. Friedmann, N.A. Missert, M.P. Siegal, J.P. Sullivan, Raman spectroscopy of amorphous carbon 498, MRS Online Proceeding Library Archive, 1998.

[49] F. Tuinstra, J.L. Koenig, Raman spectrum of graphite, J. Chem. Phys. 53 (1970) 1126.

[50] D. Wang, R. Yu, Y. Chen, N. Kumada, N. Kinomura, M. Takano, Photocatalysis property of needle-like TiO2 prepared from a novel titanium glycolate precursor, Solid State Ionics 172 (2004) 101–104.

[51] R.G. Chaudhary, H.D. Juneja, R. Pagadala, N.V. Gandhare, M.P. Gharpure, Synthesis, characterization and thermal degradation behaviour of some coordination polymers by using TG–DTG and DTA techniques, J. Saudi Chem. Soc. 19 (2015) 442–453.